Research article

Journal of Molecular Recognition

Received: 20 April 2015, Revised: 30 July 2015, Accepted: 2 August 2015, Published online in Wiley Online Library: 3 September 2015

(wileyonlinelibrary.com) DOI: 10.1002/jmr.2495

Biotinylation of the Fcγ receptor ectodomains by mammalian cell co-transfection: application to the development of a surface plasmon resonance-based assay

July Dorion-Thibaudeau[a,b], Gilles St-Laurent[b], Céline Raymond[b,c], Gregory De Crescenzo[a]* and Yves Durocher[b,c]**

We here report the production of four biotinylated Fcγ receptor (FcγR) ectodomains and their subsequent stable capture on streptavidin-biosensor surfaces. For receptor biotinylation, we first describe an *in-cell* protocol based on the co-transfection of two plasmids corresponding to one of the FcγR ectodomains and the BirA enzyme in mammalian cells. This strategy is compared with a standard sequential *in vitro* enzymatic biotinylation with respect to biotinylation level and yield. Biotinylated FcγR ectodomains that have been prepared with both strategies are then compared by analytical ultracentrifugation and surface plasmon resonance (SPR) analyses. Overall, we demonstrate that *in-cell* biotinylation is an interesting alternative to standard biotinylation protocol, as it requires less purification steps while yielding higher titers.

Finally, biotin-tagged FcγRs produced with the *in-cell* approach are successfully applied to the development of SPR-based assays to evaluate the impact of the glycosylation pattern of monoclonal antibodies on their interaction with CD16a and CD64. In that endeavor, we unambiguously observe that highly galactosylated trastuzumab (TZM-gal), non-glycosylated trastuzumab (TZM-NG), and reference trastuzumab are characterized by different kinetic profiles upon binding to CD16a and CD64 that had been captured at the biosensor surface via their biotin tag. More precisely, while TZM-NG binding to CD16a was not detected, TZM-gal formed a more stable complex with CD16a than our reference TZM. In contrast, both glycosylated TZM bound to captured CD64 in a stable and similar fashion, whereas the interaction of their non-glycosylated form with CD64 was characterized by a higher dissociation rate.

Keywords: FcγR; BirA enzyme; biotin acceptor peptide (BAP); monoclonal antibody; glycosylation; surface plasmon resonance

INTRODUCTION

Fcγ receptors (FcγRs) are transmembrane proteins divided in three types, based on their interactions with immunoglobulin G (IgG) and structural attributes. While different variants of the type III (FcγRIIIa/b or CD16a/b) and type II (FcγRIIa-c or CD32a-c) receptors have been found, the type I receptor (FcγRI or CD64) is unique (Powell and Hogarth, 2008). Immunoreceptor tyrosine-based inhibition and activation motifs (ITIM and ITAM, respectively), present in the intracellular domain of the FcγRs, are involved in signaling after receptor activation. Signaling through ITAM receptors (i.e., CD16a, CD32a, and CD64) results in cell activation, while that from ITIM receptors (i.e., CD32b) is inhibitory (Male *et al*., 2007). CD32 and CD16 are considered to be low-affinity receptors with K_Ds for the Fc region of monoclonal antibodies (Mabs) of ~10^{-5}–10^{-7} M (Radaev and Sun, 2002; Lu *et al*., 2011). In contrast, CD64 presents a higher affinity for Mabs (K_D of 10^{-8}–10^{-10} M), more likely because of the presence of a third binding domain in its extracellular portion (Lu *et al*., 2011). CD16a and CD64 are known to bind to IgGs with a 1:1 stoichiometry (Kato *et al*., 2000; Radaev and Sun, 2001; Pollastrini *et al*., 2011) but for CD32, the stoichiometry remains unclear. That is, crystallographic results by Sonderman and colleagues have pointed towards a 2:1 stoichiometry (Sondermann *et al*., 1999), whereas other experiments (analytical ultracentrifugation

* *Correspondence to: G. De Crescenzo, Department of Chemical Engineering, Groupe de Recherche en Sciences et Technologies Biomédicales, Bio-P2 Research Unit, École Polytechnique de Montréal, P.O. Box 6079, succ. Centre-ville, Montreal, QC, Canada, H3C 3A7.*
E-mail: gregory.decrescenzo@polymtl.ca

** *Y. Durocher, Département de biochimie et médecine moléculaire, Faculté de médecine, Université de Montréal, Montreal, QC, Canada, H3C 3J7.*
E-mail: yves.durocher@cnrc-nrc.ca

a *J. Dorion-Thibaudeau, G. De Crescenzo*
Department of Chemical Engineering, Groupe de Recherche en Sciences et Technologies Biomédicales, Bio-P2 Research Unit, École Polytechnique de Montréal, P.O. Box 6079, succ. Centre-ville, Montreal, QC, Canada, H3C 3A7

b *J. Dorion-Thibaudeau, G. St-Laurent, C. Raymond, Y. Durocher*
Human Health Therapeutics Portfolio, National Research Council Canada, Montreal, QC, Canada, H4P 2R2

c *C. Raymond, Y. Durocher*
Département de biochimie et médecine moléculaire, Faculté de médecine, Université de Montréal, Montreal, QC, Canada, H3C 3 J7

and asymmetrical flow field flow fractionation) tend to be indicative of a 1:1 interaction (Kato *et al*., 2000; Pollastrini *et al*., 2011).

Monoclonal antibodies have been used as therapeutic agents for many years now. The most widely used Mabs belong to the IgG family, being characterized by an ~150-kDa molecular weight and composed of two cysteine-bound heavy and light chains. When an IgG targets a cell-surface antigen, its Fc domain engages immune cells through interactions with FcγRs expressed at their surface. This, in turn, activates the effector functions of the immune system, such as the antibody-dependent or the complement-dependent cellular cytotoxicity (ADCC or CDC). The interactions between FcγRs and IgGs are thus often of critical importance to achieve a therapeutic effect and they can be positively or negatively modulated. Of salient interest, many studies have reported how glycosylation of the Fc domain of IgG influences the interactions with these receptors (Okazaki *et al*., 2004; Jefferis, 2005; Shibata-Koyama *et al*., 2009; Houde *et al*., 2010). For example, the absence of glycosylation on the Asn297 residue of the heavy chain is known to abrogate IgG interactions with CD16a and CD64 (Walker *et al*., 1989; Leader *et al*., 1991; Krapp *et al*., 2003) while the lack of a core fucose in the Fc glycan increases IgG affinity for CD16a (Shields *et al*., 2002; Scallon *et al*., 2006; Houde *et al*., 2010; Ferrara *et al*., 2011). The same observation has been made with bisecting *N*-Acetylglucosamine (GlcNac), most likely as it reduces the level of fucosylation (Umana *et al*., 1999). On the same note, high levels of sialylation were shown to reduce ADCC activity (Scallon *et al*., 2007), whereas Mabs presenting increased levels of galactosylation have been shown to interact with CD16a with higher affinity (Houde *et al*., 2010; Dorion-Thibaudeau *et al*., 2014).

The therapeutic effect of a given antibody may thus be improved by enriching recombinant IgG bearing specific glycan structures. This can be achieved by manipulating several bioprocess parameters such as the production cell line, the medium composition, the cell culture conditions, and the downstream processing, or alternatively, by *in-cell* or *in vitro* glycan remodeling (Durocher and Butler, 2009; Spearman *et al*., 2011; Raymond *et al*., 2012). Because the glycosylation profile of a given Mab may vary from batch to batch, it is important to assess it. As the glycosylation profile of therapeutic Mabs influences their interactions with Fcγ receptors, surface plasmon resonance (SPR) assays based on the use of the ectodomain of these receptors may be of most interest to evaluate their quality. Our latest study in which a His-tag capture of CD16a and CD64 had been investigated, revealed however that an anti-His antibody-mediated capture might introduce kinetic artifacts (Dorion-Thibaudeau *et al*., 2014). Therefore, we have chosen to investigate the appropriateness and the potential benefits of another approach relying on the strong interaction between biotin and streptavidin in order to capture the receptor ectodomain onto the biosensor surface in a more stable and oriented manner.

We first here explored the production of site-specific biotin-tagged FcγR ectodomains. Our biotinylated receptor production strategy relied on the co-transfection of mammalian cells with plasmids encoding an FcγR ectodomain fused to a biotin acceptor peptide (BAP) and the BirA enzyme. This approach that will be hereafter referred to as *in-cell* biotinylation was compared with the *in vitro* enzymatic biotinylation using recombinant BirA for biotinylation level and overall receptor yields. The resulting biotinylated FcγRs were then tested for the development of SPR assays aiming at evaluating IgGs with various glycosylation patterns.

MATERIALS AND METHODS

Fcγ receptor ectodomain production

Plasmids and DNA

The codon-optimized sequence encoding the human ectodomain of CD16a (residues 1 to 193) linked to a Tobacco Etch Virus nuclear inclusion a endopeptidase (TEV protease) cleavage site followed by a histidine tag was previously synthesized (GeneArt) and cloned into the pTT5 vector. The resulting plasmid pTT5-CD16aTEVHis was digested with *Bam*HI and *Age*I to remove the TEV cleavage site and replace it by insertion of a linker encoding the BAP, giving the final plasmid pTT5-CD16aBapHis. The codon-optimized sequences encoding the human ectodomain of CD32a (residues 1 to 206), CD32b (residues 1 to 216), and CD64a (residues 1 to 289) were synthesized by GeneArt, digested with *Eco*RI and *Bam*HI, and cloned into pTT5-CD16aBapHis digested with the same enzyme to remove the CD16a sequence to generate pTT5-CD32aBapHis, pTT5-CD32bBapHis, and pTT5-CD64aBapHis plasmids, respectively. The optimized sequence encoding the secreted BirA enzyme (residues 1 to 359 in-frame with the bovine prolactin signal peptide) was synthesized (GeneArt) and cloned into pTT5 vector resulting in the plasmid pTT5-BirA. The pTTo-GFPq plasmid has been described elsewhere (Durocher *et al*., 2002).

Mammalian cell culture

The human embryonic kidney 293 cell line, stably expressing truncated EBNA1 protein (HEK293-6E), was cultured in suspension using FreeStyle 17™ medium (Life Technologies, Burlington, ON, Canada) supplemented with 4 mM of glutamine, 25 μg/ml of geneticin, and 0.1% (v/v) of Kolliphor® P 188 (Sigma) in a humidified incubator at 37 °C with 5% CO_2. The Chinese hamster ovary cell line expressing a truncated EBNA1 protein (CHO-3E7) (Raymond *et al*., 2012) was cultured in the same medium but without geneticin supplementation.

Co-transfection protocol

To determine the amount of BirA plasmid needed for the production of biotin-tagged FcγRs, six different DNA ratios were used for transient transfection. HEK293-6E (CD16a; CD32a; CD32b) or CHO-3E7 (CD64) cells were first distributed in 6-well plates at 1.9×10^6 cells/ml in 1.8 ml medium. For the low affinity receptors, transfection mixtures were then prepared as follows: 2 μg of plasmids (25% w/w pTT5-CD16BapHis or pTT5-CD32a(b) BapHis, 5% pTTo-GFP, 0–3% pTT5-BirA, and 70–67% ssDNA) were diluted in 100 μl F17 medium, and 100 μl F17 medium containing 6 μg of 25 kDa linear PEI was added. For the high affinity receptor, transfection mixtures were prepared as follows: 2 μg of plasmids (50% w/w pTT5-CD64BapHis, 15% pTT22-AKT-DD, 5% pTTo-GFP, 0–3% pTT5-BirA, and 30–27% ssDNA) were diluted in 100 μl F17 medium, and 100 μl F17 medium containing 10 μg of polyethylenimine max (PEImax; Polysciences, Warrington, PA, USA) was added. The mixtures were immediately vortexed and incubated for 5 min (or 15 min for CD64) at room temperature prior to addition to the cells. One day post-transfection (dpt), TN1 peptone was added to the cell suspension in order to reach a final concentration of 0.5% (w/v) for CD16a, CD32a, and CD32b. For CD64a, cells were fed with TN1 peptone 1% (w/v) and valproic acid (1 mM) at 1 dpt and the temperature was shifted

to 32 °C to enhance protein production (Furukawa and Ohsuye, 1998; Sunley *et al*., 2008).

Western blot analysis

Samples were loaded with sodium dodecyl sulfate (SDS) onto a non-reducing polyacrylamide gel electrophoresis (SDS-PAGE) after 5 dpt. Proteins were transferred to a 0.2-μm Protran® nitrocellulose membrane (Schleicher & Schuell, USA) using Tris-glycine as a buffer for 1 h at 300 mA. The membranes were incubated 30 min in blocking reagent (Roche Diagnostics, Indianapolis, IN, USA) and then probed with streptavidin-HRP (BD Bioscience, Mississauga, ON, Canada) or anti-histidine-HRP (Sigma-Aldrich, Oakville, ON, Canada) for 1 h. Detection was performed using BM Chemiluminescence Blotting Substrate (Roche Diagnostics) and a Gel Doc™ imaging system (Bio-Rad, Mississauga, ON, Canada).

Production and purification

Scale-up production of the CD32a, CD32b, and CD64 receptors was performed using 500-ml cell cultures in 2-l shake flasks at 120 rpm with 3% (w/w) BirA plasmid. For CD16a, two batches were produced. The transfections were performed as described earlier using 0% and 3% (w/w) BirA plasmid (no biotinylation and *in-cell* biotinylation, respectively). For each culture, the ectodomain was purified 5 dpt by immobilized metal-affinity chromatography (IMAC) as described by Tom and colleagues (Tom *et al*., 2008), and aggregates removal was performed by preparative SEC as described elsewhere (Dorion-Thibaudeau *et al*., 2014). Purified receptors were quantified by absorbance at 280 nm using a Nanodrop™ spectrophotometer (Thermo Fisher Scientific, Madison, WI, USA) based on their respective molar extinction coefficients. SDS-PAGE was performed by adapting the protocol described by Boucher and colleagues (Boucher *et al*., 2008).

In vitro biotinylation

Purified non-biotinylated CD16a-BAP ectodomain was used for BirA mediated *in vitro* biotinylation. The enzymatic reaction was performed using the BirA-500 kit following the manufacturer recommendations (Avidity, Aurora, CO, USA). Briefly, the biotinylation was performed at 37 °C for 2 h by mixing CD16a-BAP (50 μM, 1.6 ml), Biomix-A (200 μl), Biomix-B (200 μl), and BirA enzyme (20 μl). Purification of the ectodomain and aggregate removal were carried out as mentioned earlier.

Biotinylation quantification of the various Fcγ receptor pools

The percentage of biotinylation was determined using Pierce® Avidin Agarose beads (Thermo Scientific, Rockford, IL, USA) by indirect measurement. Biotin-saturated beads were obtained by mixing 25 μl of D-biotin (500 μM, Avidity, Aurora, CO, USA) with 50 μl of avidin beads (50% (v/v)). To remove the excess of biotin, the bead slurry was washed three times in phosphate buffered saline. The beads (Avi) and the biotin-saturated beads (Avi-B) were then individually mixed with 0.3 μg of FcγR for 15 min and then centrifuged at 500 × g for 1 min, in duplicates. The supernatants were loaded onto a non-reducing Mini-PROTEAN® TGX Stain-Free™ SDS-PAGE (Bio-Rad, Mississauga, ON, Canada) and the intensity of the bands corresponding to CD16a (*I*) was measured with the Image Lab software (Bio-Rad). This procedure allowed for the calculation of the percentage of biotinylation according to the equation:

$$Biotinylation\ (\%) = \frac{(I_{Avi-B} - I_{Avi})}{I_{Avi-B}} *100$$

Immunoglobulin G production

For this study, Trastuzumab (TZM), a humanized mouse IgG1 was selected as our reference antibody. Non-glycosylated TZM (TZM-NG) corresponded to a modified TZM where the Fc N-glycosylation site was eliminated by mutating Asparagine 297 to a Glutamine. TZM and TZM-NG were produced by transient co-expression of the heavy and light chains in CHO-3E7 (Raymond *et al*., 2012). TZM glycoform being enriched in galactose (TZM-gal) was obtained by co-expressing of the human beta 1,4-galactosyltransferase (Raymond *et al*., accepted manuscript). Antibody purification and aggregate removal were performed as described elsewhere (Dorion-Thibaudeau *et al*., 2014).

Glycosylation profile analysis

Trastuzumab glycoforms analysis was performed by trypsin and PNGaseF digestions followed by a matrix-assisted laser desorption ionization mass spectrometry (MALDI-MS) assay as previously described (Dorion-Thibaudeau *et al*., 2014). As expected, mass spectrometry analysis of the various glycan pools corresponding to our different versions of TZM confirmed the expected differences in N-glycan profiles and were in agreement with previously reported profiles corresponding to other TZM samples we had prepared according to the same protocols (Dorion-Thibaudeau *et al*., 2014).

Analytical ultracentrifugation analysis

Sedimentation velocity analyses were performed using a Proteomelab XL-I analytical ultracentrifuge (Beckman Coulter, Fullerton, CA, USA). Runs were carried out using two-channel centerpieces (Beckman Coulter) and an eight-hole AN50 Ti analytical rotor pre-equilibrated to 25.0 °C. The assay was conducted with an absorbance detection at 280 nm, a radial scan increment of 0.003 cm, an angular velocity of 50 000 rpm, and a temperature of 25.0 °C. The data were analyzed by applying the continuous c(s) distribution model in SEDFIT (version 14.3e). The bottom position was fixed to 7.2 cm but the meniscus and frictional ratio varied as fitted parameters. The sedimentation coefficient range was set between 0 and 15 with a confidence level (F-ratio) of 0.68. The corresponding figure (Figure 3) was generated with the GUSSI software (version 1.0.8d).

Surface plasmon resonance analysis

All surface plasmon resonance (SPR) experiments were performed using a Biacore T100 instrument (GE Healthcare) at a flow rate of 50 μl/min at 25 °C using HBS-P 1×, pH 7.4 (GE Healthcare) as running buffer. Kinetic analysis was performed with the Biacore T100 Evaluation software. The Biotin CAPture kit (GE Healthcare) was used to stably capture biotinylated FcγR at the surface of the biosensor, according to manufacturer recommendations. The CAP chip (included with the kit) consisted of carboxymethylated dextran surface pre-coated with single-stranded DNA (ssDNA). The procedure consisted of a first capture that was performed by

injecting a macromolecular complex composed of a complementary ssDNA attached to a streptavidin (≈3500 response unit (RU)). Biotin-tagged low affinity receptors were captured over the streptavidin surface at a flow rate of 10 μl/min for 1 min (0.5 μg/ml, 100 RU), and CD64 was captured using the same flow rate for 45 s (0.1 μg/ml, 40 RU) while no receptor was injected over the reference surface. Mab solutions were then injected over captured CD16a, CD32a, CD32b (10, 30, 100, 300, 500, 1000 nM, 2 min), and CD64 (1, 3, 10, 30, 100 nM, 1 min) and control surfaces. The receptor/IgG dissociation was monitored by injecting running buffer for 5 min or 12 min for CD64. Surface regeneration (dissociation of complementary ssDNA-streptravidin from the ssDNA surface) was performed by injecting the regeneration solution included with the kit (6 M guanidine-HCl, 0.25 M NaOH). Data were double-referenced prior analysis (Myszka, 1999).

RESULTS

In-cell biotinylation of Fcγ receptors by co-transfection of BirA in mammalian cells

Plasmids corresponding to the BirA enzyme and to the extracellular portion of CD16a, CD32a, CD32b, or CD64, all tagged with the BAP sequence in addition to 10 histidine residues at their C-terminus, were used to produce biotin-tagged FcγR ectodomains by transient co-transfection of mammalian cells. For co-transfection, different ratios of BirA plasmid within the co-transfection mix were tested (1–3% (w/w)) to define the amount needed in order to get the best compromise between receptor production and biotinylation. For all tested conditions, the supernatants were collected 5 dpt and run on non-reducing SDS-PAGE gels, which were then analyzed by Western blots using anti-histidine-horseradish peroxidase (HRP) antibody and streptavidin-HRP as probes (Figure 1). For CD16a and CD64, each supernatant was characterized by the presence of a smear that most likely corresponded to aggregates (the molecular weight of monomeric CD16a and CD64 was calculated to be around 25 and 35 kDa, respectively, without taking biotinylation and glycosylation into account). The anti-histidine probe revealed that the addition of BirA plasmid in the DNA preparation decreased the overall receptor production level (Figure 1 panels A1–C1). Western blots corresponding to the use of streptavidin as a probe showed no band when the BirA plasmid had not been added in the transfection mix, as expected because this enzyme is absolutely needed for BAP biotinylation (Beckett *et al*., 1999) (Figure 1, panels A2–C2). In contrast to decreasing FcγRs expression when increasing BirA plasmid amounts (as observed with the anti-histidine-HRP probe), levels of FcγR biotinylation were higher when increasing BirA plasmid level up to 3% (as detected with the streptavidin-HRP probe). The presence of 3% (w/w) of BirA plasmid was thus considered to be the optimal condition for the production of biotinylated receptors because this amount allowed obtaining a high level of biotinylation without decreasing drastically the overall production yield (significant decrease in Fc receptors expression was observed with higher BirA plasmid percentages—data not shown). This experimental condition was then selected for larger-scale (500 ml) production, which was followed by receptor purification by IMAC. Non-reducing SDS-PAGE gels were run with samples corresponding to each purification step (Figure 2). The last step (size-exclusion chromatography (SEC)) yielded an almost pure monomeric form for all receptors as a single band was observed on the gel, matching the molecular weights of the monomeric FcγRs. For CD32a, a light band around 25 kDa was also observed, which likely corresponded to the non-glycosylated form of the receptor (Figure 2B). The overall yields of purified CD16a, CD32a/b, and CD64 and their percentage of biotinylation (determined with a commercial assay kit relying on the use of avidin beads) are given in Table 1.

Influence of the biotinylation method on CD16a yields

Because the addition of the BirA plasmid to the transfection mix decreased the yield of total CD16a expression and, to some

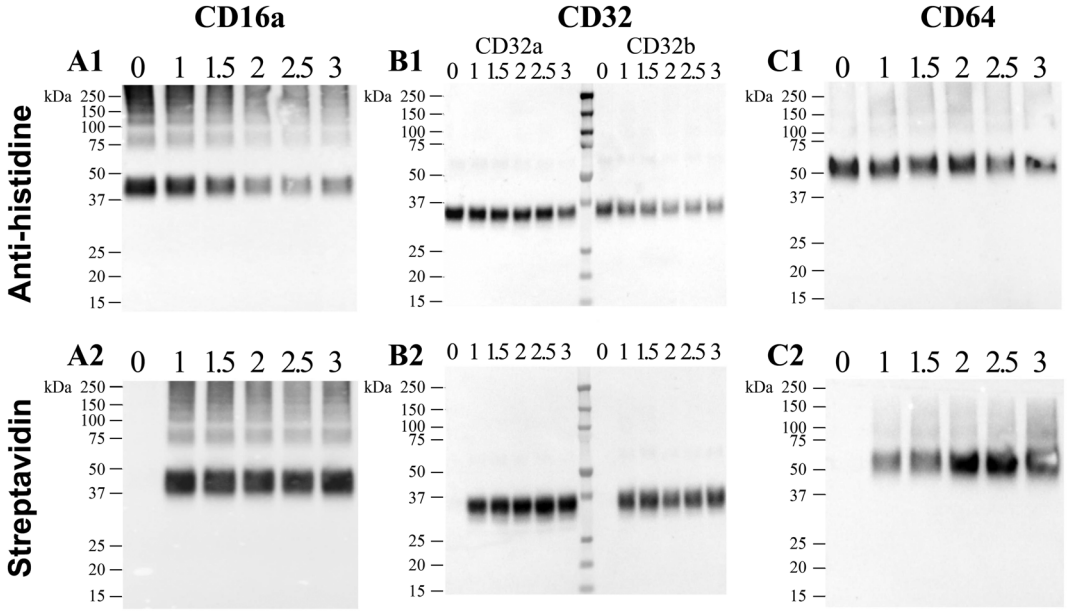

Figure 1. Western blots of supernatants corresponding to CD16a (A), CD32a (B), CD32b (B), and CD64 (C) using 0–3% (w/w) BirA plasmid, probed with either anti-histidine (1) for total receptor production or streptavidin (2) for biotinylation level.

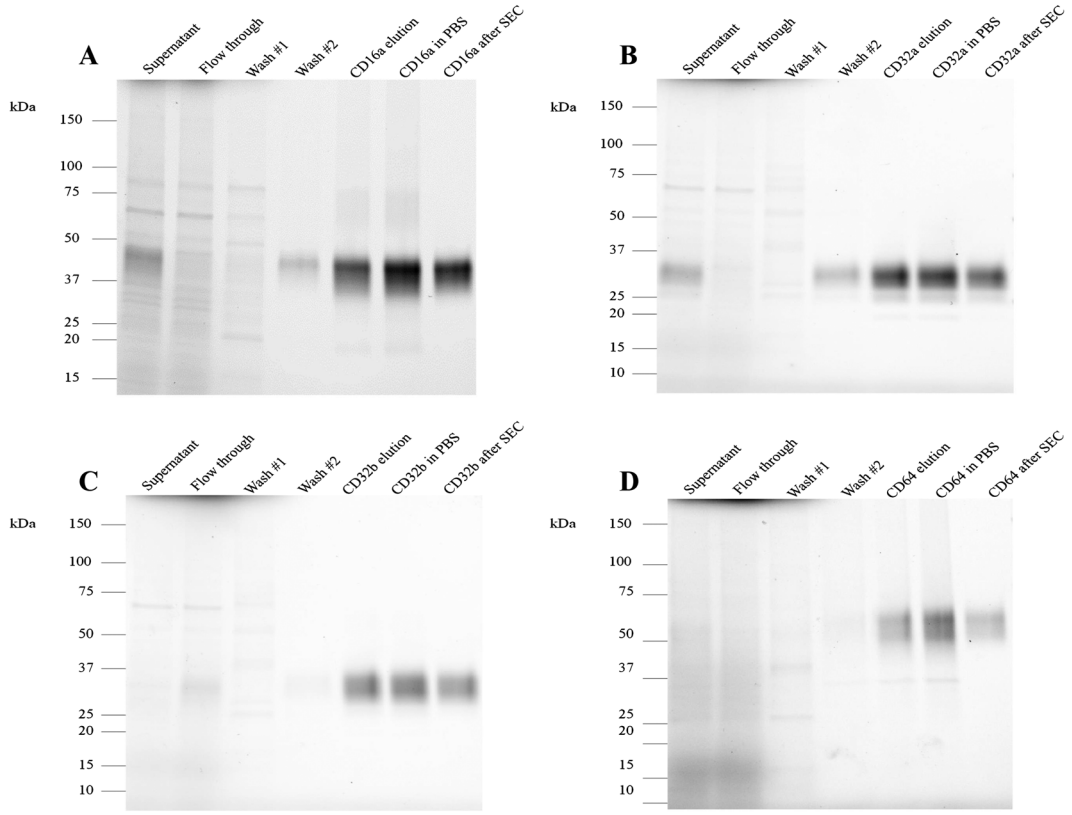

Figure 2. Coomassie staining of non-reducing sodium dodecyl sulfate polyacrylamide gel electrophoresis gels corresponding to the production of biotinylated CD16a (A), CD32a (B), CD32b (C), and CD64 (D) ectodomains. 18 µl of sample corresponding to each purification step were loaded while 2–3 µg of proteins from the elution, phosphate-buffered saline (PBS) wash, and size-exclusion chromatography (SEC) pool aliquots were loaded onto the gel.

Table 1. CD16a production: final titers post-purification and biotinylation levels

	Titer (mg/l culture)	Biotinylation (%)
CD16a *no biotin*	15.9	—
In-cell CD16a	13.9	88
In vitro CD16a	9.4	78
In-cell CD32a	12.0	68
In-cell CD32b	4.6	72
In-cell CD64	0.6	64

extent that of other receptor ectodomains (Figure 1, panels A1–C1), we next evaluated the utility of the co-transfection approach by comparing it with a standard *in vitro* enzymatic biotinylation protocol using commercially available BirA (latter designated as the *in vitro* protocol in this manuscript). That is, we first produced and affinity purified BAP-tagged CD16a; the purified protein was then biotinylated *in vitro* by addition of BirA and its substrate. The mixture was then passed on an IMAC column to separate the biotinylated protein from the BirA enzyme and unreacted substrate. The biotinylation levels were 88% and 78% and the titers were 13.9 mg and 9.4 mg per liter of medium for the *in-cell* approach and *in vitro* approach using 20 µg of BirA enzyme (200 000 units), respectively (Table 1). Very similar results were obtained when additional production runs were performed (data not shown).

Analytical ultracentrifugation (AUC) analysis was carried out for both *in-cell* and *in vitro* biotinylated and non-biotinylated CD16a-BAP receptors. The c(s) distributions indicated that each CD16a preparation had very similar sedimentation coefficient, as all three peaks overlapped (Figure 3). Furthermore, the analysis of the AUC experiments indicated that all purified (IMAC + SEC) CD16a preparations contained approximately 2% of dimers.

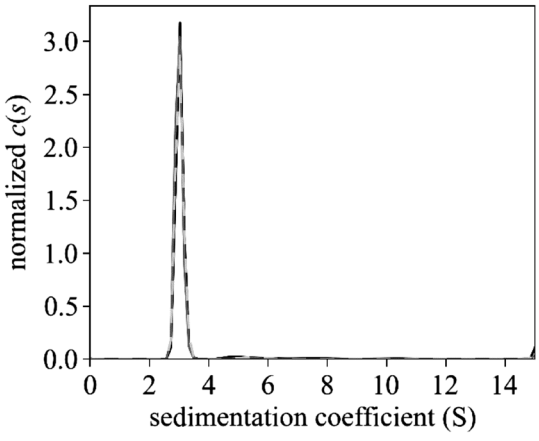

Figure 3. Sedimentation coefficient distribution of *in-cell* (black), *in vitro* (gray), and biotin-free (dashed gray) CD16a at 50 000 rpm.

Journal of Molecular Recognition

Surface plasmon resonance kinetics experiments

Because our goal was to develop a high-throughput SPR assay to characterize the interactions between FcγRs and antibodies harboring various glycosylation patterns, our strategy was to immobilize the receptor ectodomains onto several biosensor surfaces. Our approach relied on the tethering of a sensor surface-bound streptavidin for the subsequent stable capture of the biotinylated FcγR ectodomain in an oriented fashion.

Based on this strategy, real-time monitoring of the interactions between CD16a and TZM was achieved by performing duplicate injections of TZM at concentrations ranging from 10 to 1000 nM. A first series of experiments was conducted with biotinylated CD16a that was produced by *in-cell* co-transfection. As can be seen in Figure 4, the baseline was stable before the injection of the analyte, and, at the end of the dissociation, the signal went back to 0 RU. This indicated that the capture of the biotinylated receptor via streptavidin was very stable and that the CD16a/IgG complex dissociated within less than 300 s. Moreover, duplicate injections were practically superimposed, thus further validating the approach, more specifically, the reproducibility of the streptavidin and receptor ectodomain captures. For comparison with values reported in the literature, global fit (Figure 4) and steady-state affinity analyses (inset in Figure 4) of the resulting sensorgrams were performed, assuming a Langmuirian 1:1 interaction (Table 2). The same protocol was then applied to compare both versions of biotinylated CD16a (corresponding to *in-cell* or *in vitro* biotinylation). As can be seen in Figure 5, the injection of 1000 nM of TZM over both receptor surfaces gave identical normalized sensorgrams (duplicates injections), which suggested that the biotinylation protocol did not influence the ability of the biotinylated receptor to interact with a given IgG.

The same SPR strategy was used to monitor CD64/TZM interactions. Mab injections with concentrations ranging between 1 and 100 nM were performed in duplicate as seen in Figure 6. For each sensorgram, the baseline was stable before analyte injection, thus indicating a stable CD64 capture via previously captured streptavidin. A global fit of the sensorgrams was performed assuming 1:1 interaction (Figure 6, Table 3).

Finally, the same capture approach was applied to biotinylated CD32a-BAP and CD32b-BAP, following which, injections of TZM at concentrations ranging from 10 to 1000 nM were performed (Figure 7, duplicate injections). Again, the capture of the biotinylated receptor ectodomains on the streptavidin surface was observed to be very stable before analyte injection for both CD32a (Figure 7A) and CD32b (Figure 7B). As expected for both receptors, the interactions with TZM were characterized by fast association and dissociation rates. Therefore, steady-state analysis only was performed for each set of sensorgrams in order to estimate the thermodynamic dissociation constant of each interaction (insets in Figure 7, Table 3).

The SPR assays corresponding to the oriented capture of biotinylated CD16a and CD64 by means of a previously tethered

Table 2. Kinetics parameters related to the interactions of CD16a with reference trastuzumab (Figure 4)

	Global fit (1:1)	Steady-state affinity (1:1)
k_a ($M^{-1}\,s^{-1}$)	$(2.94 \pm 0.03) \times 10^4$	—
k_d (s^{-1})	$0.03 \pm 1.50 \times 10^{-4}$	—
K_D (M)	$(1.02 \pm 0.02) \times 10^{-6}$	$(2.29 \pm 0.27) \times 10^{-6}$
R_{max} (RU)	90.7 ± 0.7	272 ± 23
χ^2	0.313	0.928

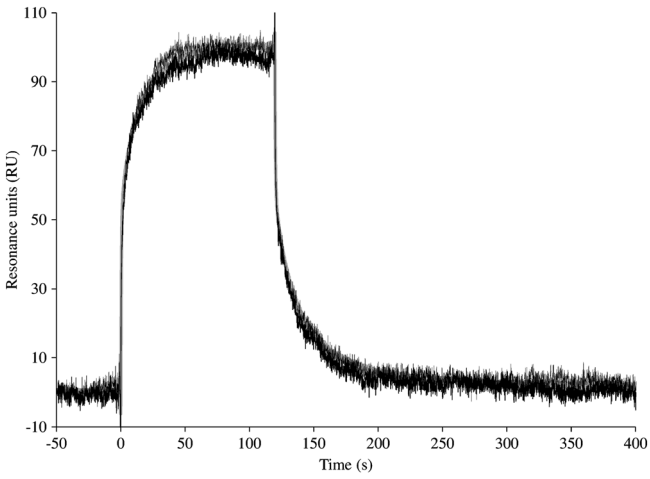

Figure 5. Sensorgrams corresponding to the injection of trastuzumab at 1000 nM over *in-cell* (black) and *in vitro* (gray) CD16a, both in duplicates.

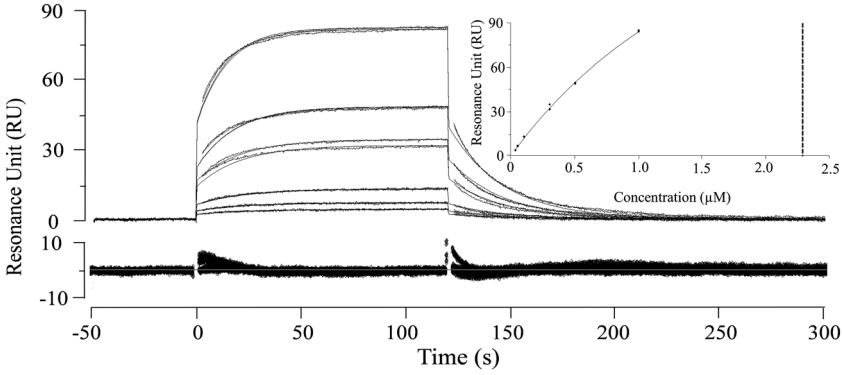

Figure 4. Sensorgrams corresponding to the interactions between injected control trastuzumab (10, 30, 100, 300, 500, 1000 nM, duplicate injections) and biotinylated CD16a that had been captured by streptavidin. Double-referenced sensorgrams were globally fit (corresponding residuals shown in the bottom panel) and a steady-state analysis was also performed (inset) both assuming a 1:1 simple model interaction. Note that in the inset, the vertical dashed line corresponds to the K_D value derived from the steady-state analysis.

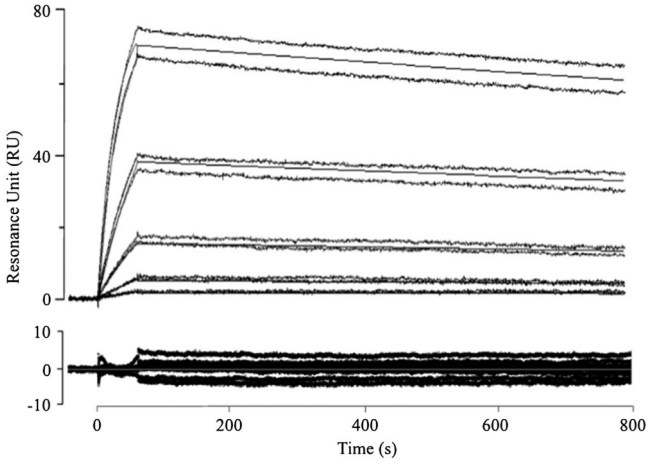

Figure 6. Sensorgrams corresponding to the interactions between reference trastuzumab (1, 3, 10, 30, 100 nM, duplicate injections) and biotinylated CD64 captured by streptavidin. Double-referenced sensorgrams were globally fit assuming 1:1 simple model (corresponding residuals shown in the bottom panel).

Table 3. Kinetic and thermodynamic parameters related to the interactions of CD32a, CD32b, and CD64 with reference trastuzumab (Figures 6 and 7)

	CD32a	CD32b	CD64
	Steady-state affinity (1:1)		Global fit (1:1)
k_a (M^{-1} s^{-1})	—	—	$(3.63 \pm 0.01) \times 10^5$
k_d (s^{-1})	—	—	$(1.98 \pm 0.03) \times 10^{-4}$
K_D (M)	$(0.60 \pm 0.03) \times 10^{-6}$	$(1.66 \pm 0.24) \times 10^{-6}$	$(0.55 \pm 0.06) \times 10^{-9}$
R_{max} (RU)	77.7 ± 1.9	140 ± 13	80.1 ± 0.1
χ^2	0.309	0.823	3.86

streptavidin at the biosensor surface were also evaluated for their ability to detect differences within TZM glycosylation profiles. In that endeavor, injections of our reference TZM, in addition to TZM-gal (a TZM preparation containing high galactosylation levels, that is, 11% G1F and 66% G2F while G0F was found at 5% by hydrophilic interaction chromatography (HILIC), data not shown) and TZM-NG (a mutated TZM that is not glycosylated) (Dorion-Thibaudeau *et al*., 2014) were performed. Duplicate injections of each of these TZM preparations were performed at 1000 nM over a streptavidin-bound CD16a surface (Figure 8A) or at 300 nM over a streptavidin-bound CD64 surface (Figure 8B). Double-referenced normalized sensorgrams are shown in Figure 8. Of interest, the different TZM glycoforms interacting with CD16a were characterized by different dissociation profiles: dissociation of the IgG/CD16a complexes was complete only after 250 and 300 s for TZM and TZM-gal, respectively. As expected, TZM-NG did not interact with CD16a. In the case of immobilized CD64, TZM-NG binding to CD64 was observed: the kinetics corresponding to the aglycosylated Mab were however strikingly different from those observed with our reference glycosylated TZM. For TZM-gal, similar binding to that of the reference TZM was observed when interacting with CD64.

DISCUSSION

In-cell biotinylation of Fcγ receptors

We here report for the first time an efficient biotinylation protocol applied to Fcγ receptor ectodomains. This protocol relies on the transient co-transfection of mammalian cells with two distinct plasmids: one corresponding to the secreted BirA enzyme and the other to the protein of interest being fused at its C-terminus to a BAP sequence. We demonstrated that this approach was advantageous when compared with the standard *in vitro* biotinylation procedure, as the latter requires both FcγR and BirA enzyme to be purified, while additional affinity purification is necessary to remove BirA and reaction components from the biotinylated receptor preparation.

In-cell biotinylation has been previously described in several research articles using a single vector coding for both the secreted BirA enzyme and the protein of interest (Predonzani *et al*., 2008; Viens *et al*., 2008). That methodology, however, does not permit to fine-tune the ratio between BirA and the protein of interest; based on our current observations, these amounts need to be adjusted for optimal performance (Figure 1). It is more likely that the optimal ratio of BirA/BAP-tagged protein will depend on the protein to be biotinylated; these adjustments would be uneasy to perform with a single-vector strategy.

Biotin-free and *in-cell* biotinylated receptor were produced at the 500-ml culture scale (with 0% and 3% BirA plasmid, respectively) and subsequently purified to obtain monomeric CD16a ectodomains (Figure 2A). Biotin-free CD16a was then used as a substrate for *in vitro* biotinylation to compare the final overall titer, the percentage of biotinylation, the sedimentation coefficient (by AUC) and the kinetics of binding to TZM—our reference antibody for this study (by SPR). While biotinylation levels were found to be similar for the *in-cell* and *in vitro* approaches (Table 1), the final receptor yield was higher for the *in-cell* strategy, making it very attractive when considering all other advantages mentioned earlier. A comparison of the c(s) distribution profiles of both biotin-tagged and non-biotinylated CD16a highly suggests that the biotinylation methodologies do not influence the conformation of the protein (Figure 3). This hypothesis is further reinforced by our SPR results indicating that both ectodomains, once captured via their biotin tag, yield identical kinetic profiles for TZM binding (Figure 5). Altogether our results indicate that the *in-cell* biotinylation protocol, compared to a typical *in vitro* biotinylation, is advantageous as it is faster (less purification steps) and cost-effective, while giving significantly higher yields (Table 1) for the same product bioactivity.

Surface plasmon resonance assay development

The use of SPR biosensors has been reported by many research groups as a relevant tool to evaluate the kinetic constants of IgG/FcγR interactions. Among these studies, the variety of experimental protocols that were reported (choice of the partner to be immobilized or captured, flow rates and densities) yielded to inconsistencies among reported kinetic values (Galon *et al*., 1997; Li *et al*., 2007; Bruhns *et al*., 2009; Luo *et al*., 2009; Magistrelli *et al*., 2012). In many cases, kinetic profiles were observed to deviate from a simple Langmuirian model. These deviations can be attributed to the intrinsic complexity of the biological interactions under study (e.g., heterogeneity within the glycosylation of the antibody and/or receptor preparations) or suboptimal experimental procedures (mass transfer limitation, crowded

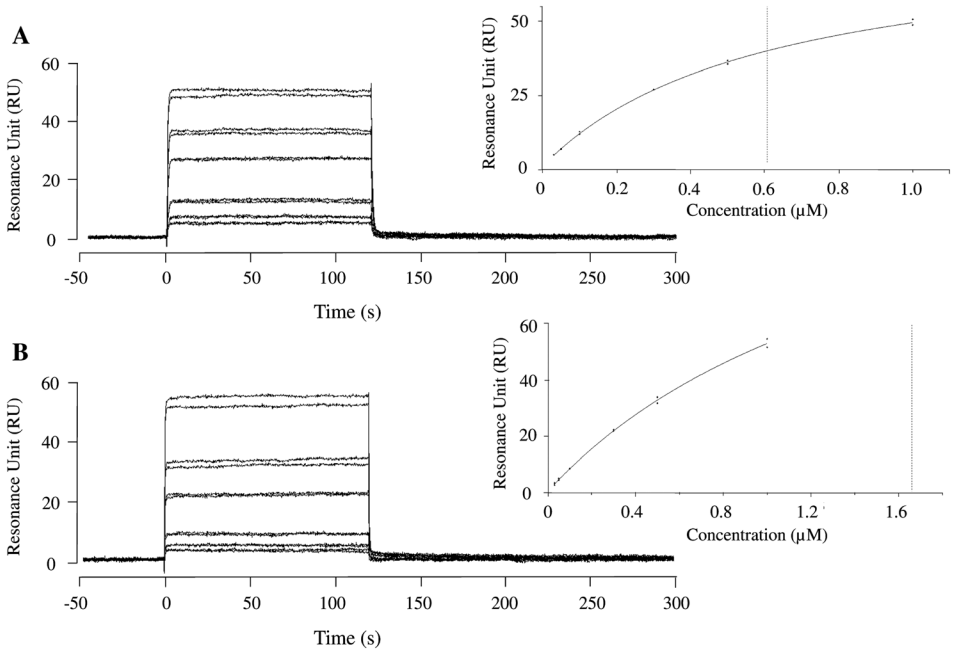

Figure 7. Sensorgrams corresponding to the interactions between reference trastuzumab (10, 30, 100, 300, 500, 1000 nM, duplicate injections) and biotinylated CD32a (A) or CD32b (B) captured by streptavidin. Double-referenced sensorgrams were analyzed by a steady-state analysis (see insets). Note that in the insets, the vertical dashed lines correspond to the K_D values derived from the steady-state analyses.

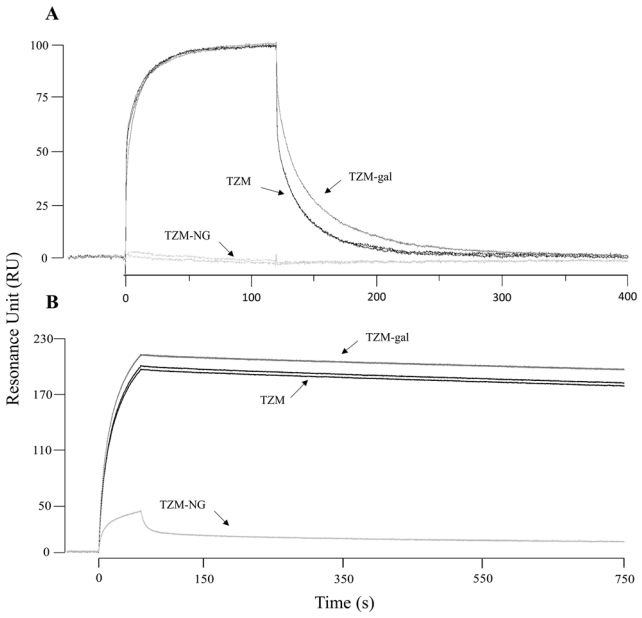

Figure 8. Sensorgrams corresponding to the injection of reference trastuzumab (TZM) (black), TZM-NG (light gray), TZM-gal (dark gray) at 1000 nM over CD16a (A) or at 300 nM over CD64 (B), in duplicates. TZM-NG, non-glycosylated trastuzumab; TZM-gal, highly galactosylated trastuzumab.

surfaces, heterogeneous ligand orientation…) that have been extensively discussed by the members of the SPR community over the years (Myszka, 1999; Magistrelli *et al*., 2012). We have shown in a previous study that the oriented capture of CD16a significantly affects its binding kinetics when compared with the same ectodomain being randomly immobilized, most likely because the random immobilization approach resulted in heterogeneous receptor populations at the biosensor surface (Dorion-Thibaudeau *et al*., 2014). In that study, the oriented capture of CD16a was mediated by His-tagged CD16a binding to an anti-His antibody that had been previously immobilized at the SPR biosensor surface. This capture protocol was however shown to have its own weaknesses. That is, a yet unexplained transient maximum followed by a decrease (rather than a stable plateau) was observed during the injection phase of our reference TZM over captured CD16a (Figure 9). Such an atypical behavior was also observed by others (Luo *et al*., 2009; Zeck *et al*., 2011). Moreover, the anti-histidine capture approach we tested was not suitable for CD64 because, at high TZM concentrations, the response signal was negative at the end of the dissociation phase (Figure 9). We postulated at that time that such phenomena could be due to the fact that antibody binding to FcγR might weaken the anti-His antibody/FcγR interaction or, alternatively, that the anti-His antibody competed with the injected antibody for FcγR binding. We reasoned that, in either case, changing our capture strategy to an approach relying on a strong interaction that does not involve any antibody might solve the issues and thus allow for a better kinetic characterization. This motivated the biotin capture presented here as a robust alternative to the use of a His-tag capture antibody. To our knowledge, this experimental approach has never been reported for the capture of FcγRs.

Higher flow rate as well as low receptor densities were used in SPR biosensing experiments in order to avoid any mass transport/rebinding artifacts (Myszka, 1999) while antibody aggregates were removed prior to antibody injection because we demonstrated that as little as 2% of aggregate within an antibody preparation may significantly affect the kinetic profile of the antibody/CD16a interactions (Dorion-Thibaudeau *et al*., 2014). As expected, the biotin/streptavidin capture approach we developed lead to the recording of sensorgrams in which the atypical sensorgram shape that had been previously observed for CD16a was not recorded (Figure 9). This assay is thus a significant improvement to the His-tag capture protocols that has been commonly used up to now (Luo *et al*., 2009; Zeck

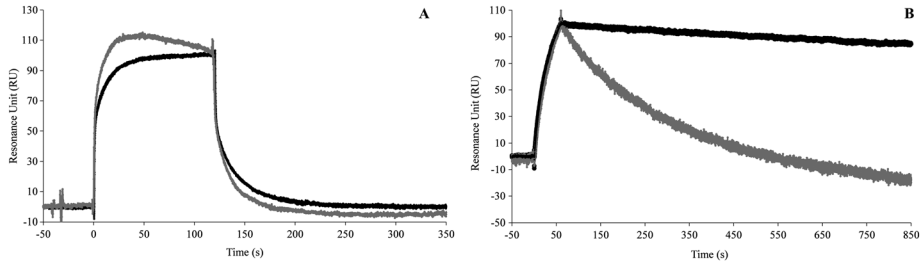

Figure 9. Normalized sensorgrams corresponding to the injection of 1000 nM of control trastuzumab over CD16a (A) or CD64 (B) that had been captured via a his-tag protocol (Dorion-Thibaudeau *et al*., 2014) (gray curves) or via biotin-streptavidin interactions (black curves, this study).

et al., 2011; Dorion-Thibaudeau *et al*., 2014). A global analysis of the SPR data corresponding to CD16a interactions with TZM (Figure 4) was performed to determine the kinetic constants, and thus calculate the apparent thermodynamic dissociation constant (K_D) of the interaction. In spite of all the precautions we took to eliminate any unwanted artifacts that may bias our kinetic interpretation of the data, the CD16a interactions with TZM were still observed to deviate from a simple model, as one can deduce from visual inspection (Figure 4). This deviation is thus most likely due to the fact that TZM glycosylation was not homogenous in the preparation, as determined by mass spectrometry (Dorion-Thibaudeau *et al*., 2014). Each TZM subpopulation may thus be characterized by a distinct set of kinetic constants when interacting with CD16a. This hypothesis is supported by our SPR results corresponding to TZM harboring different glycosylation profiles (see succeeding paragraphs).

Since we reached equilibrium at the end of each TZM injection (plateau), a steady-state analysis was also performed to determine the apparent K_D of the interaction (inset in Figure 4). The latter was twofold larger than the one calculated by the ratio of the kinetic rates (global fit, Table 2). A threefold difference was also observed for the R_{max} values that were determined with both approaches, highly suggesting that these observed discrepancies are due to the fact that the TZM concentrations we injected were too low for an accurate R_{max} and K_D determination by a steady-state analysis. However, it is important to note that the apparent K_D, emanating from both global fit and steady-state analyses (Table 2) are within the same order of magnitude as those previously reported (Radaev and Sun, 2002; Lu *et al*., 2011; Dorion-Thibaudeau *et al*., 2014).

The biotin capture approach has also improved the quality of the sensorgrams corresponding to the interaction between CD64 and TZM. The observed classical shape is indeed contrasting with our previous results corresponding to the anti-His CD64 capture strategy (negative net responses were observed during the dissociation phase, Figure 9). A global analysis of the sensorgrams corresponding to CD64 interaction with TZM (Figure 6) was performed to determine the kinetic constants of the interactions, and calculate the apparent thermodynamic dissociation constant (K_D, Table 3). The latter is also in agreement with values from the literature (Lu *et al*., 2011; Patel *et al*., 2013).

Kinetic experiment using CD32a and CD32b interacting with TZM were also performed with this new capture protocol (Figure 7). Once again, the transient maximum we previously observed with the anti-His capture approach (unreported results) were absent. The fast rates of the interactions in both the analyte and buffer injection phases lead us to evaluate the K_D of the interaction using a steady-state type of analysis only (Table 3). Again, we obtained values that are in agreement with the literature (Maenaka *et al*., 2001). TZM injections at higher concentrations would however be needed for a more accurate (K_D, R_{max}) determination for these receptors because apparent K_Ds were in both cases close or higher than the maximal concentration of TZM we injected (Figure 7).

Of interest, in spite of the deviations from a simple kinetic model we observed with captured CD16a and CD64 (via biotin/streptavidin interactions), both ectodomains were proven to be valuable to distinguish various glycoforms of TZM based on a visual inspection of their binding kinetics (more precisely, differences in the dissociation profiles, Figure 8), in excellent agreement with the literature (Walker *et al*., 1989; Leader *et al*., 1991; Krapp *et al*., 2003; Houde *et al*., 2010; Dorion-Thibaudeau *et al*., 2014). On that note, according to the results reported in Figure 8, Mab binding to CD16a and CD64 receptor ectodomains is impacted in a different fashion depending on Mab glycosylation profile. The simultaneous use of distinct surfaces displaying streptavidin-captured CD16a and CD64 may thus provide a good semi-quantitative analysis of the glycoprofile of a given pool of Mabs by SPR. That is, while the dissociation profiles recorded on CD16a surfaces may allow for the detection of different Mab glycoforms (as observed for highly galactosylated and reference Mabs, Figure 8A), the CD64 surface is efficient in detecting aglycosylated Mabs within a given pool because their dissociation profile strikingly contrasts with those of glycosylated Mabs (Figure 8B). Our group is currently working at generating a larger panel of Mab glycoforms in order to correlate their SPR kinetic signature when interacting with FcγR ectodomains (this assay) to their therapeutic efficacy as evaluated in *in vitro* cell assays.

CONCLUSION

We have developed an efficient protocol for *in-cell* protein biotinylation by transient BirA co-transfection in mammalian cells that we successfully applied to the CD16a, CD32a, CD32b, and CD64 ectodomains. This innovative methodology is faster and yields similar biotinylation level compared with a typical *in vitro* biotinylation. Biotin-tagged FcγRs were subsequently used for the development of SPR surfaces to perform real-time monitoring interactions with Mabs. Our results demonstrated that, even with an optimized experimental setup, CD16a still exhibits complex kinetics of interactions with Mabs, more likely due to heterogeneity within the pools of Mabs we tested. Nevertheless, the biotin tag capture approach we here report is promising for the setup of SPR assays aiming at assessing the glycosylation profile of the Mab. These SPR assays may be used as part of a high-throughput routine for quality control/characterization in a Mab screening platform in order to predict Mab therapeutic efficacy.

Journal of Molecular Recognition

Acknowledgements

The authors would like to thank Louis Bisson, Brian Cass, and Christian Gervais for their help with protein production and purification at NRC and also Erika Lattová and Dr. Hélène Perreault (University of Manitoba) for glycosylation analysis. This work was supported by the NSERC Strategic Network for The Production of Single-type Glycoform Monoclonal Antibodies (MabNet) group.

REFERENCES

Beckett, D, Kovaleva, E, Schatz, PJ. 1999. A minimal peptide substrate in biotin holoenzyme synthetase-catalyzed biotinylation. *Proc. Natl. Acad. Sci. U. S. A.* **8**(4): 921–929.

Boucher, C, St-Laurent, G, Loignon, M, Jolicoeur, M, De Crescenzo, G, Durocher, Y. 2008. The bioactivity and receptor affinity of recombinant tagged EGF designed for tissue engineering applications is defined by the nature and position of the tags. *Tissue Eng. Part A* **14**(12): 2069–2077.

Bruhns, P, Iannascoli, B, England, P, Mancardi, DA, Fernandez, N, Jorieux, S, Daeron, M. 2009. Specificity and affinity of human Fcgamma receptors and their polymorphic variants for human IgG subclasses. *Blood* **113**(16): 3716–3725.

Dorion-Thibaudeau, J, Raymond, C, Lattova, E, Perreault, H, Durocher, Y, De Crescenzo, G. 2014. Towards the development of a surface plasmon resonance assay to evaluate the glycosylation pattern of monoclonal antibodies using the extracellular domains of CD16a and CD64. *J. Immunol. Methods* **408**: 24–34.

Durocher, Y, Perret, S, Kamen, A. 2002. High-level and high-throughput recombinant protein production by transient transfection of suspension-growing human 293-EBNA1 cells. *Nucleic Acids Res.* **30**(2E9.): .

Durocher, Y, Butler, M. 2009. Expression systems for therapeutic glycoprotein production. *Curr. Opin. Biotechnol.* **20**(6): 700–707.

Ferrara, C, Grau, S, Jaeger, C, Sondermann, P, Bruenker, P, Waldhauer, I, Hennig, M, Ruf, A, Rufer, AC, Stihle, Mand others. 2011. Unique carbohydrate-carbohydrate interactions are required for high affinity binding between Fc gamma RIII and antibodies lacking core fucose. *Proc. Natl. Acad. Sci. U. S. A.* **108**(31): 12669–12674.

Furukawa, K, Ohsuye, K. 1998. Effect of culture temperature on a recombinant CHO cell line producing a C-terminal alpha-amidating enzyme. *Cytotechnology* **26**(2): 153–164.

Galon, J, Robertson, MW, Galinha, A, Mazieres, N, Spagnoli, R, Fridman, WH, Sautes, C. 1997. Affinity of the interaction between Fc gamma receptor type III (Fc gammaRIII) and monomeric human IgG subclasses. Role of Fc gammaRIII glycosylation. *Eur. J. Immunol.* **27**(8): 1928–1932.

Houde, D, Peng, Y, Berkowitz, SA, Engen, JR. 2010. Post-translational modifications differentially affect IgG1 conformation and receptor binding. *Mol. Cell. Proteomics* **9**(8): 1716–1728.

Jefferis, R. 2005. Glycosylation of recombinant antibody therapeutics. *Biotechnol. Prog.* **21**(1): 11–16.

Kato, K, Sautès-Fridman, C, Yamada, W, Kobayashi, K, Uchiyama, S, Kim, H, Enokizono, J, Galinha, A, Kobayashi, Y, Fridman, WHand others. 2000. Structural basis of the interaction between IgG and fc[gamma] receptors. *J. Mol. Biol.* **295**(2): 213–224.

Krapp, S, Mimura, Y, Jefferis, R, Huber, R, Sondermann, P. 2003. Structural analysis of human IgG-Fc glycoforms reveals a correlation between glycosylation and structural integrity. *J. Mol. Biol.* **325**(5): 979–989.

Leader, KA, Kumpel, BM, Hadley, AG, Bradley, BA. 1991. Functional interactions of aglycosylated monoclonal anti-D with Fc gamma RI+ and Fc gamma RIII+ cells. *Immunology* **72**(4): 481–485.

Li, P, Jiang, N, Nagarajan, S, Wohlhueter, R, Selvaraj, P, Zhu, C. 2007. Affinity and kinetic analysis of Fcgamma receptor IIIa (CD16a) binding to IgG ligands. *J. Biol. Chem.* **282**(9): 6210–6221.

Lu, J, Ellsworth, JL, Hamacher, N, Oak, SW, Sun, PD. 2011. Crystal structure of Fcgamma receptor I and its implication in high affinity gamma-immunoglobulin binding. *J. Biol. Chem.* **286**(47): 40608–40613.

Luo, Y, Lu, Z, Raso, SW, Entrican, C, Tangarone, B. 2009. Dimers and multimers of monoclonal IgG1 exhibit higher in vitro binding affinities to Fcgamma receptors. *MAbs* **1**(5): 491–504.

Maenaka, K, van der Merwe, PA, Stuart, DI, Jones, EY, Sondermann, P. 2001. The human low affinity Fcgamma receptors IIa, IIb, and III bind IgG with fast kinetics and distinct thermodynamic properties. *J. Biol. Chem.* **276**(48): 44898–44904.

Magistrelli, G, Malinge, P, Anceriz, N, Desmurs, M, Venet, S, Calloud, S, Daubeuf, B, Kosco-Vilbois, M, Fischer, N. 2012. Robust recombinant FcRn production in mammalian cells enabling oriented immobilization for IgG binding studies. *J. Immunol. Methods* **375**(1–2): 20–29.

Male, DK, Roitt, Y, Brostoff, J. 2007. Immunologie. Elsevier Masson: ISSY LES MOULINEAUX (France).

Myszka, DG. 1999. Improving biosensor analysis. *J. Mol. Recognit.* **12**(5): 279–284.

Okazaki, A, Shoji-Hosaka, E, Nakamura, K, Wakitani, M, Uchida, K, Kakita, S, Tsumoto, K, Kumagai, I, Shitara, K. 2004. Fucose depletion from human IgG1 oligosaccharide enhances binding enthalpy and association rate between IgG1 and Fc gamma RIIIa. *J. Mol. Biol.* **336**(5): 1239–1249.

Patel, R, Johnson, KK, Andrien, BA, Tamburini, PP. 2013. IgG subclass variation of a monoclonal antibody binding to human Fc-gamma receptors. *Am. J. Biochem. Biotechnol.* **9**(3): 206–219.

Pollastrini, J, Dillon, TM, Bondarenko, P, Chou, RYT. 2011. Field flow fractionation for assessing neonatal Fc receptor and Fc gamma receptor binding to monoclonal antibodies in solution. *Anal. Biochem.* **414**(1): 88–98.

Powell, MS, Hogarth, PM. 2008. Fc Receptors. Multichain Immune Recognition Receptor Signaling: From Spatiotemporal Organization to Human Disease. Springer-Verlag Berlin: Berlin. pp 24–34.

Predonzani, A, Arnoldi, F, Lopez-Requena, A, Burrone, OR. 2008. In vivo site-specific biotinylation of proteins within the secretory pathway using a single vector system. *BMC Biotechnol.* **8**: 41.

Radaev, S, Sun, P. 2002. Recognition of immunoglobulins by Fc[gamma] receptors. *Mol. Immunol.* **38**(14): 1073–1083.

Radaev, S, Sun, PD. 2001. Recognition of IgG by Fc gamma receptor - The role of Fc glycosylation and the binding of peptide inhibitors. *J. Biol. Chem.* **276**(19): 16478–16483.

Raymond C, Robotham A, Kelly J, Lattová E, Perreault Hln, Durocher Y. 2012. Production of highly sialylated monoclonal antibodies. Glycosylation, Dr. Petrescu S (ed). ISBN: 978-953-51-0771-2, InTech, doi:10.5772/51301.

Scallon, BJ, Tam, SH, McCarthy, SG, Cal, AN, Raju, TS. 2007. Higher levels of sialylated Fc glycans in immunoglobulin G molecules can adversely impact functionality. *Mol. Immunol.* **44**(7): 1524–1534.

Scallon, BJ, Snyder, LA, Anderson, GM, Chen, Q, Yan, L, Weiner, LM, Nakada, MT. 2006. A review of antibody therapeutics and antibody-related technologies for oncology. *J. Immunother.* **29**(4): 351–364.

Shibata-Koyama, M, Iida, S, Okazaki, A, Mori, K, Kitajima-Miyama, K, Saitou, S, Kakita, S, Kanda, Y, Shitara, K, Kato, K and others. 2009. The N-linked oligosaccharide at Fc gamma RIIIa Asn-45: an inhibitory element for high Fc gamma RIIIa binding affinity to IgG glycoforms lacking core fucosylation. *Glycobiology* **19**(2): 126–134.

Shields, RL, Lai, J, Keck, R, O'Connell, LY, Hong, K, Meng, YG, Weikert, SHA, Presta, LG. 2002. Lack of fucose on human IgG1 N-linked oligosaccharide improves binding to human FcγRIII and antibody-dependent cellular toxicity. *JBC* **277**(30): 26733–26740.

Sondermann, P, Huber, R, Jacob, U. 1999. Crystal structure of the soluble form of the human fcgamma-receptor IIb: a new member of the immunoglobulin superfamily at 1.7 A resolution. *EMBO J.* **18**(5): 1095–1103.

Spearman, M, Dionne, B, Butler, B. 2011. Chapter 12: The Role of Glycosylation in Therapeutic Antibodies. Antibody Expression and Production. Springer: Dordrecht, New York.

Sunley, K, Tharmalingam, T, Butler, M. 2008. CHO cells adapted to hypothermic growth produce high yields of recombinant beta-interferon. *Biotechnol. Prog.* **24**(4): 898–906.

Tom, R, Bisson, L, Durocher, Y. 2008. Purification of His-tagged proteins using fractogel-cobalt. *Cold Spring Harb. Protoc.* **2008**(3pdb.prot4980): 1–4.

Umana, P, Jean-Mairet, J, Moudry, R, Amstutz, H, Bailey, JE. 1999. Engineered glycoforms of an antineuroblastoma IgG1 with optimized antibody-dependent cellular cytotoxic activity. *Nat. Biotechnol.* **17**(2): 176–180.

Viens, A, Harper, F, Pichard, E, Comisso, M, Pierron, G, Ogryzko, V. 2008. Use of protein biotinylation in vivo for immunoelectron microscopic localization of a specific protein isoform. *J. Histochem. Cytochem.* **56**(10): 911–919.

Walker, MR, Lund, J, Thompson, KM, Jefferis, R. 1989. Aglycosylation of human IgG1 and IgG3 monoclonal antibodies can eliminate recognition by human cells expressing Fc gamma RI and/or Fc gamma RII receptors. *Biochem. J.* **259**(2): 347–353.

Zeck, A, Pohlentz, G, Schlothauer, T, Peter-Katalinic, J, Regula, JT. 2011. Cell type-specific and site directed N-glycosylation pattern of FcgammaRIIIa. *J. Proteome Res.* **10**(7): 3031–3039.

